ACS NANO
Cite This: ACS Nano 2017, 11, 10616-10622
www.acsnano.org

ARTICLE

Rod-Like Virus-Based Multiarm Colloidal Molecules

Alexis de la Cotte,‡ Cheng Wu,‡ Marie Trévisan, Andrii Repula, and Eric Grelet*

Centre de Recherche Paul-Pascal, CNRS, and Université de Bordeaux, 115 Avenue Schweitzer, 33600 Pessac, France

Supporting Information

ABSTRACT: We report on the construction of multiarm colloidal molecules by tip-linking filamentous bacteriophages, functionalized either by biological engineering or chemical conjugation. The affinity for streptavidin of a genetically modified vector phage displaying Strep-tags fused to one end of the viral particle is measured by determining the dissociation constant, K_d. In order to improve both the colloidal stability and the efficiency of the self-assembly process, a biotinylation protocol having a chemical yield higher than 90% is presented to regioselectively functionalize the cystein residues located at one end of the bacteriophages. For both viral systems, a theoretical comparison is performed by developing a quantitative model of the self-assembly and interaction of the modified viruses with streptavidin compounds, which accurately accounts for our experimental results. Multiarm colloidal structures of different valencies are then produced by conjugation of these tip-functionalized viruses with streptavidin activated nanoparticles. We succeed to form stable virus-based colloidal molecules, whose number of arms, called valency, is solely controlled by tuning the molar excess. Thanks to a fluorescent labeling of the viral arms, the dynamics of such systems is also presented in real time by fluorescence microscopy.

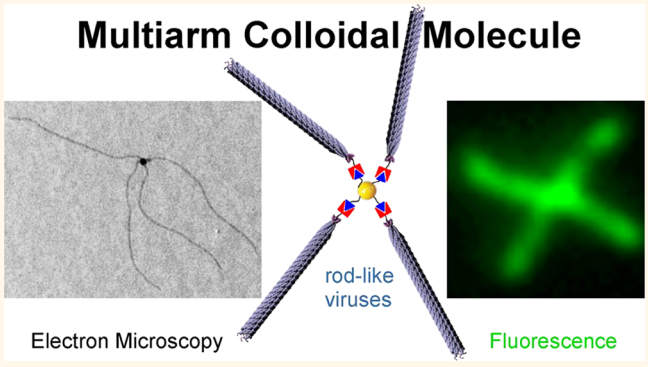

KEYWORDS: *self-assembly, M13 bacteriophage, nanorod, hybrid, colloidal molecule, tunable valency, star polymer*

The design of structured materials at the mesoscopic scale is a challenge that can be addressed with two main strategies usually referred as top-down and bottom-up approaches.[1,2] While the top-down methods consist in the elaboration of patterns and in their progressive size reduction, the bottom-up approach requires the use of nano- or microscaled building blocks for which the self-assembly can be driven by entropic or enthalpic contributions allowing for producing hierarchical architectures.[3] Specifically, most of reported studies have focused on sphere-based assemblies with specific sizes and/or functionalizations opening the field of so-called "colloidal molecules".[4−6] To go beyond the spherical symmetry and developing more complex architectures, some investigations have been performed using nanorods as elementary building blocks.[7−11] Mainly two distinct paths have been considered for creating multiarm colloidal molecules: the core-first and the arm-first approaches. In the former case, the core is a multivalent initiator from which the arms can be grown. In this way, multivalent-branched nanocrystals[12] or polymer stars can be obtained by a specific crystal growth or by the polymerization of monomers around the core.[13−19] This method allows for a control over the length and/or the width of each constituent but limits the construction of objects to a specific valency and a tailored size. The second approach consists in the self-assembly of linear constituents into multivalent star- or flower-like structures. This technique requires an end-to-end assembly of the particles which can be achieved in different ways such as DNA templating,[20,21] amphiphilic interactions,[22−24] biorecognition,[7,9,25−27] or tip-linking reaction of linear polymer chains.[28,29] In this paper, we focus on the end-to-end self-assembly of filamentous viruses and aim to obtain multiarm structures of tunable valency (*i.e.*, variable number of arms). Such viral rod-like particles can be seen both as elementary building blocks monodisperse in size and shape and as versatile scaffolds for biological engineering and chemical functionalization of their coat proteins.[30−32] Prior studies have reported the use of bacteriophages, mainly modified by phage display, that self-assemble into chains of various length,[25,33] rings,[34] or radial structures.[9,10] These works are based on the genetic engineering of viruses with mutated tip proteins (minor proteins p3 and p9, corresponding respectively to the two extremities of the phage) onto which specific polypeptidic sequences are fused. The formation of chains or rings is then driven either by the complementarity of the

Received: September 8, 2017
Accepted: September 21, 2017
Published: September 21, 2017

DOI: 10.1021/acsnano.7b06405
ACS Nano 2017, 11, 10616−10622

involved polypeptidic sequences[25] or by the introduction of an external cross-linker.[34] Star-like structures were also achieved by using the affinity of biotin for streptavidin[10] or by biorecognition of a specific motif histidine-proline-glutamine (HPQ),[35] called Strep-tag, with streptavidin-coated nanoparticles (NPs).[9] Specifically, a mutant called M13-AntiStreptavidin (M13AS), initially isolated through the screening of a phage display library, has been already used in templating hierarchically organized hybrid materials.[9,36,37] Here, we study this M13AS mutant displaying Strep-tags at one end by first quantifying its affinity for streptavidin with the determination of its dissociation constant in solution, K_d. Because of the relatively high dissociation constant K_d found, limiting therefore the self-assembly efficiency for the formation of colloidally stable multiarm structures, we have developed a chemical alternative approach based on the biotinylation of cystein residues present at one tip (p3 proteins) of the so-called M13C7C bacteriophages. The protocol relies on the thiol-based bioconjugation, and it has been optimized to be both highly specific (no other coat protein modified) and efficient (yield of about 92%). We then discuss a quantitative model accounting for the interaction with streptavidin of both the biologically and the chemically functionalized phages for various initial conditions. When exposed to a dispersion of streptavidin-coated NPs, biotinylated phages self-assemble into colloidally stable multiarm structures, as the affinity of streptavidin for biotin is several orders of magnitude higher than for Strep-tags. Moreover, these multiarm molecules display a tunable valency which can be continuously monitored by varying the relative molar excess of biotinylated phages and streptavidin activated NPs. This approach makes also possible a second chemical functionalization of the phages by their body labeling with fluorescent dyes, allowing for the *in situ* observation by optical microscopy of their self-assembly into multiarm colloidal molecules.

RESULTS AND DISCUSSION

M13AS Binding Affinity and Biotinylation Yield of M13C7C-B. In our mixtures of M13 viruses (either AntiStreptavidin phages, M13AS or biotinylated phages, M13C7C-B) and streptavidin-coated NPs exhibiting q streptavidin molecules (Strep) per NP, the principle of mass conservation species provides the two following relations:

$$[\mathrm{M13}]_0 = [\mathrm{M13}]_{\mathrm{free}} + [\mathrm{M13}]_{\mathrm{bound}} \tag{1}$$

with $[\mathrm{M13}]_0$ the initial virus concentration, $[\mathrm{M13}]_{\mathrm{free}}$, and $[\mathrm{M13}]_{\mathrm{bound}}$, the respective concentrations at equilibrium of free and bound (or reacted) viruses with streptavidin-coated NPs:

$$q \times [\mathrm{NP}]_0 = (q \times [\mathrm{NP}]_{\mathrm{free}} + (q - n) \times [\mathrm{NP}]_{\mathrm{bound}}) + n \times [\mathrm{NP}]_{\mathrm{bound}} \tag{2}$$

where n is the number of viruses bound per NP ($1 \leq n \leq q$), $[\mathrm{NP}]_0$ and $[\mathrm{NP}]_{\mathrm{free}}$ are the respective initial and unreacted concentrations of NPs, and $[\mathrm{NP}]_{\mathrm{bound}}$ is the concentration of NPs conjugated with at least one M13 virus (Figure 1). The binding affinity of a ligand for a receptor is given by the dissociation constant, K_d, which results from the following equilibrium in solution:[38]

$$\mathrm{M13}_{\mathrm{free}} + \mathrm{Strep}_{\mathrm{free}} \rightleftharpoons \mathrm{M13}_{\mathrm{bound}} \tag{3}$$

and is defined as

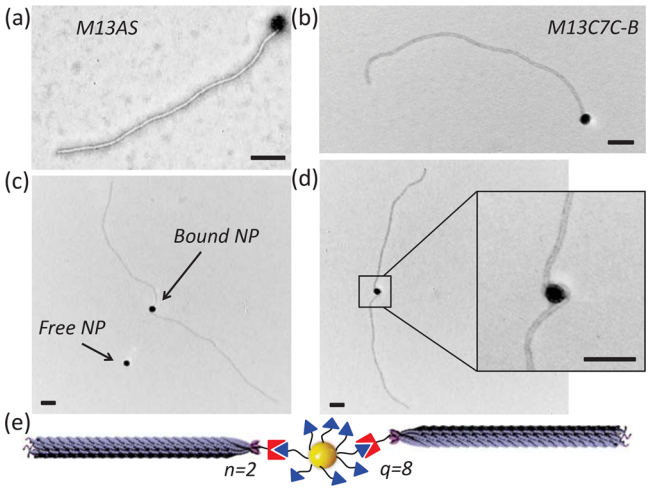

Figure 1. Transmission electron microscopy (TEM) images of M13AS (a and c) and M13C7C-B (b and d) viruses complexed with streptavidin-coated NPs. (a, b) Single viruses and (c, d) pairs of viruses bound to a NP. The scale bars represent 100 nm. (e) Schematic representation of two viruses (n = 2) bound to a NP exhibiting q = 8 streptavidin proteins at its surface.

$$K_d \equiv \frac{[\mathrm{M13}]_{\mathrm{free}} \times [\mathrm{Strep}]_{\mathrm{free}}}{[\mathrm{M13}]_{\mathrm{bound}}} \tag{4}$$

where $[\mathrm{Strep}]_{\mathrm{free}} = q \times [\mathrm{NP}]_{\mathrm{free}} + (q - n) \times [\mathrm{NP}]_{\mathrm{bound}}$. Qualitatively, the lower the K_d value is, the more stable the complex is and thus the stronger the affinity. In the case of the interaction between biotin and streptavidin protein, K_d reaches a value of 1×10^{-15} M, considered the strongest noncovalent bond found in nature.[39] The HPQ motif is a well-known Strep-tag with however a lower affinity for streptavidin than biotin, typically found in the μM range.[35] However, the affinity of M13AS phage, where the HPQ motif is displayed on each of its five p3 proteins, has not yet been determined. Using eqs 1 and 2, let us rewrite K_d as a function of an unique variable, the fraction of bound NPs $f(\mathrm{NP}) \equiv [\mathrm{NP}]_{\mathrm{bound}}/[\mathrm{NP}]_0$:

$$K_d = \left(\frac{[\mathrm{M13}]_0}{n \times f(\mathrm{NP})} - [\mathrm{NP}]_0\right) \times (q - n \times f(\mathrm{NP})) \tag{5}$$

Thanks to eq 5, the M13AS-streptavidin dissociation constant, K_d, can be determined by counting by TEM both $f(\mathrm{NP})$ and n, the average number of viruses per NP having at least one virus bound (defined also as the valency of the self-assembled structure). Note that using this model, a precise estimation of K_d can only be performed if no steric hindrance limits the binding of viruses to NPs. This means practically that $n \ll q$, as experimentally confirmed in Figure 2a,b for which $n \simeq 1.5$ (see Table 1).

As M13AS viruses are in large excess compared to NP (see Table 1), only the concentrations at equilibrium of free and bound NP as well as the average number of viruses grafted per NP, n, can been counted by TEM on a given sample ($[\mathrm{M13AS}]_{\mathrm{free}}$ being too high to be determined at the same time). In order to determine K_d, two specific mixtures of M13AS and streptavidin-coated NPs (samples **1** and **2**, described in Table 1) were realized with different initial conditions, for which the molar excess is introduced, α:

DOI: 10.1021/acsnano.7b06405
ACS Nano 2017, 11, 10616−10622

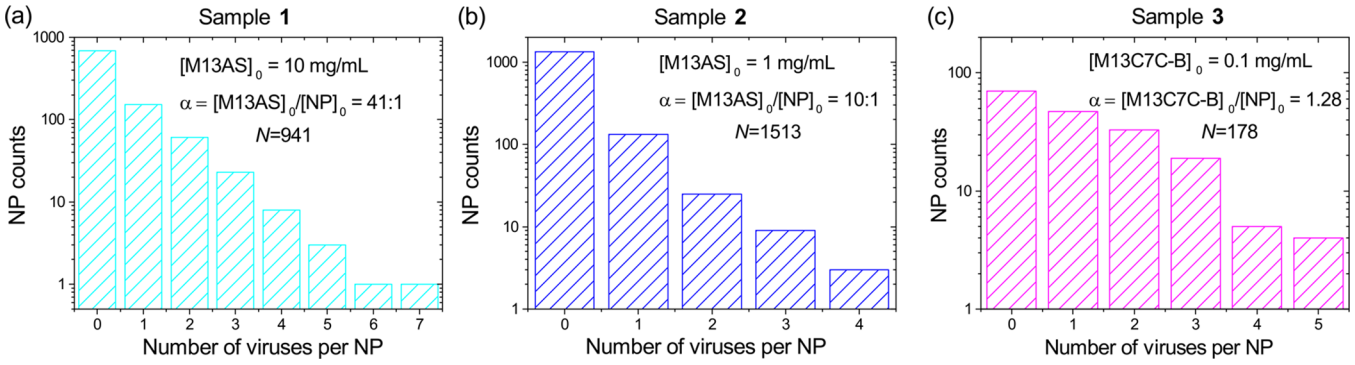

Figure 2. Distribution of the number of bound viruses per NP in suspensions of (a) M13AS at initial concentration of 10 mg/mL (5.4×10^{-7} M) with a molar excess of virus per NP $\alpha = 41$ (Sample 1), (b) $[M13AS]_0 = 1$ mg/mL (5.4×10^{-8} M) with $\alpha = 10$ (Sample 2), (c) biotinylated viruses at $[M13C7C\text{-}B]_0 = 0.1$ mg/mL (5.4×10^{-9} M) with $\alpha = 1.28$ (Sample 3). *N* indicates the total number of NP counted by TEM for establishing the statistics of each sample.

Table 1. Summary of the Experimental Conditions and Measurements Obtained by TEM for the Three Mixtures of Viruses and Streptavidin-Coated NPs[a]

Sample	1	2	3
Virus	M13AS	M13AS	M13C7C-B
$[M13]_0$ (M)	5.4×10^{-7}	5.4×10^{-8}	5.4×10^{-9}
$[NP]_0$ (M)	1.3×10^{-8}	5.4×10^{-9}	4.2×10^{-9}
$\alpha = [M13]_0/[NP]_0$	41	10	1.28
f(NP)	0.27	0.11	0.61
n	1.62	1.31	1.94
K_d (M)	9×10^{-6}	3×10^{-6}	1×10^{-15}

[a]Samples **1** and **2** correspond to biologically engineered M13AS phages and sample **3** to tip-biotinylated M13C7C-B viruses. The fraction of bound NPs, f(NP), and the average number of viruses per bead, n, result from TEM counting shown in the distributions plotted in Figure 2. The dissociation constant, K_d, is calculated for samples **1** and **2** according to eq 5, and it is taken from literature[39] for sample **3**.

$$\alpha \equiv \frac{[M13]_0}{[NP]_0} \tag{6}$$

Both mixtures were observed in TEM (Figure 1), and the distribution of the number of viruses grafted per bead is provided in Figure 2a,b for samples **1** and **2**, respectively. The mean values of n and f(NP) are deduced from these distributions, and consequently K_d is obtained thanks to eq 5. A similar dissociation constant (within the experimental margin of error) $K_d = 6\ (\pm 3) \times 10^{-6}$ M is found for both samples (Table 1). This average value is also in good agreement with the one reported in literature for the HPQ Strep-tag of about 1 μM.[35] The slightly lower binding affinity found in our case can be explained by the following reason: The determination of binding affinity is usually performed with the target compound (here: streptavidin) deposited on a solid surface, whereas our experiments were performed in bulk with dispersions of streptavidin-coated NPs. These NPs not only diffuse slower than molecular streptavidin but also induce steric hindrance as soon as some viruses are bound making more difficult further binding of other viruses. Nevertheless, this relative high value of the dissociation constant, for which $K_d \gg [M13AS]_0 \geq [NP]_0$ (Table 1), does not allow for a tight and nonreversible binding. A first alternative would be to design a Strep-tag with an affinity in the nM range, providing then a suitable efficiency for high enough initial virus (>1 mg/mL) and bead concentrations. The second alternative is to work with biotin derivatives ($K_d \simeq 1 \times 10^{-15}$ M), which have been chemically grafted at one of the virus tips (see Materials and Methods). In order to determine the biotinylation yield of the M13C7C-B phages, sample **3** has been prepared (Table 1), where phages and streptavidin activated NPs have been introduced in similar amount ($\alpha \simeq 1$,) allowing for their simultaneous counting by TEM (Figure 1). Specifically, among a total number of 229 counted viruses, 210 were bound by their tip to NPs, and 19 were found free, giving a fraction of bound M13C7C-B of f(M13) = 0.92, and therefore a yield of biotinylation of 92%. It is worth mentioning that the functionalization of the virus tips by biotin is not only efficient but also highly selective as shown by the absence of any virus-based byproducts. Moreover, the specificity of the reaction between beads and functionalized phages has been checked by a control experiment with raw M13 viruses, and, as expected no interaction is observed with NPs (see Figure S3 in the Supporting Information).

Quantitative Model for the Formation of Virus/NP Structures. Rewriting the expression of K_d given in eq 5, the fraction of bound NPs f(NP) can be accounted by the following quadratic equation:

$$f(\mathrm{NP})^2 - \frac{1}{n}\left(\frac{\alpha K_d}{[M13]_0} + q + \alpha\right) f(\mathrm{NP}) + \frac{q\alpha}{n^2} = 0 \tag{7}$$

Eq 7 can be easily solved analytically to provide f(NP) for different initial conditions. The results are plotted in Figure 3. When the binding affinity for streptavidin is low, as for M13AS viruses, the self-assembly yield to form multiarm structures ($n \geq 2$) remains weak (f(NP) < 25%), whatever the initial virus and NP concentrations (Figure 3a). At a fixed value of the dissociation constant K_d, only the initial conditions affect the equilibrium, as illustrated by the two experimental data points corresponding to samples **1** and **2**, which are in very good agreement with the predictions of the model. Figure 3b shows that strongly increasing the binding affinity favors the formation of multiarm structures, for which a total reaction can be obtained. More importantly, the valency of multiarm self-assemblies can be controlled and tuned *only* by varying the molar excess α. Finally, an outstanding agreement between our model and sample **3** is found (Figure 3b), especially considering the absence of any free parameter. In conclusion, our model quantitatively accounts for the self-assembly behavior of our two experimental systems, and it confirms that biotinylated phages are the most suitable one to form

DOI: 10.1021/acsnano.7b06405
ACS Nano 2017, 11, 10616−10622

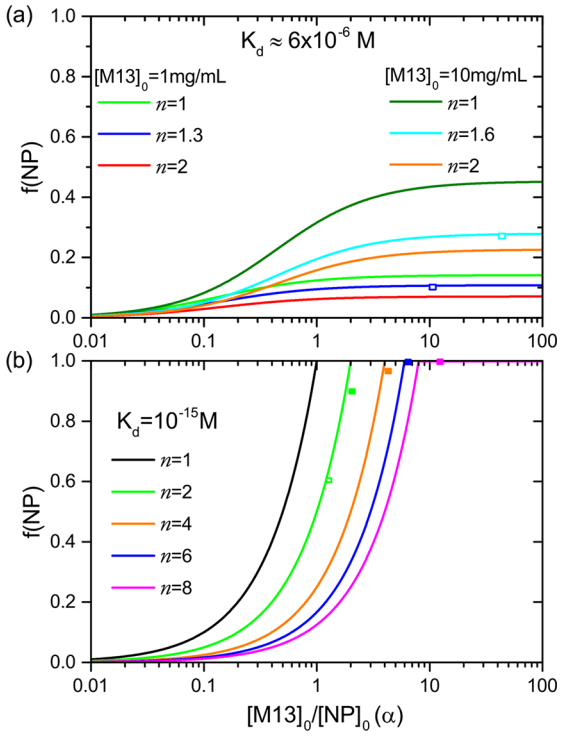

Figure 3. Fraction of bound NPs, f(NP), as modelized by eq 7, as a function of the molar excess, α, obtained for different average numbers of viruses per NP, n. Results calculated for: (a) M13AS virus strain with $K_d \simeq 6 \times 10^{-6}$ M for two different initial virus concentrations, $[M13AS]_0$; (b) biotinylated viruses, M13C7C-B, with $K_d = 1 \times 10^{-15}$ M. In this case, the results are independent of the initial virus concentration, as $[M13AS]_0 \gg K_d$, and only depend on the molar excess α. The cyan, blue, and green open square symbols represent the samples 1, 2, and 3, respectively, as described in Table 1. The green, orange, blue, and pink solid square symbols represent the four experimental samples of respective average valency n = 2.1, 4.2, 6.1, and 8.3, as reported in the next section.

multiarm colloidal molecules, as described in the next paragraph.

Construction of Multiarm Colloidal Molecules. Multiarm colloidal molecules were achieved by preparing four samples of M13C7C-B phages mixed with aqueous dispersions of streptavidin-coated NPs (see Materials and Methods). As shown in Figure 4 and Figure S4, the rod-based colloidal molecules are radial structures possessing a single central NP surrounded by up to n = 8 arms formed by tip-linked M13C7C-B functionalized phages. Figure 5 displays the increase of the average valency n of multiarm assemblies when the initial concentration of NP is decreased at a fixed virus concentration. This behavior is *quantitatively* consistent with our theoretical model, as plotted in Figure 3b where the full symbols represent the four samples of colloidal molecules reported in Figure 5. We experimentally confirm that the molar excess is the key parameter to tune the valency of the self-assemblies. After a linear increase, the average valency n saturates in Figure 5b when it reaches the maximum number of available streptavidin binding sites per bead, q. At this saturated value, n becomes independent of the initial molar excess α (for $\alpha \geq q$), as predicted by the model (Figure 3b). In the results shown in Figure 5a, all samples present a similar distribution of virus populations (except for the lowest average valency n = 2.1 which is asymmetric), whose width, defined as the standard deviation of the corresponding Gaussian fits, is $\delta n \pm 2$. This width of the average valency is narrow enough to obtain slightly polydisperse (in terms of number of arms) batches of star-like colloidal molecules for the four different prepared samples (corresponding to the four different initial NP concentrations). Thanks to an efficient and regioselective biochemical functionalization of the M13C7C phages followed by a conjugation with streptavidin activated beads, the large-scale production of multiarm structures of well-defined and tunable valency has been achieved. Furthermore, biotinylated phages are an interesting system to work with because of their ability to be twice chemically modified without losing their functionality. We have succeeded in labeling with fluorescent dyes the virus body, targeting mainly the p8 major coat proteins. Labeled M13C7C-B phages can therefore be visualized at the single

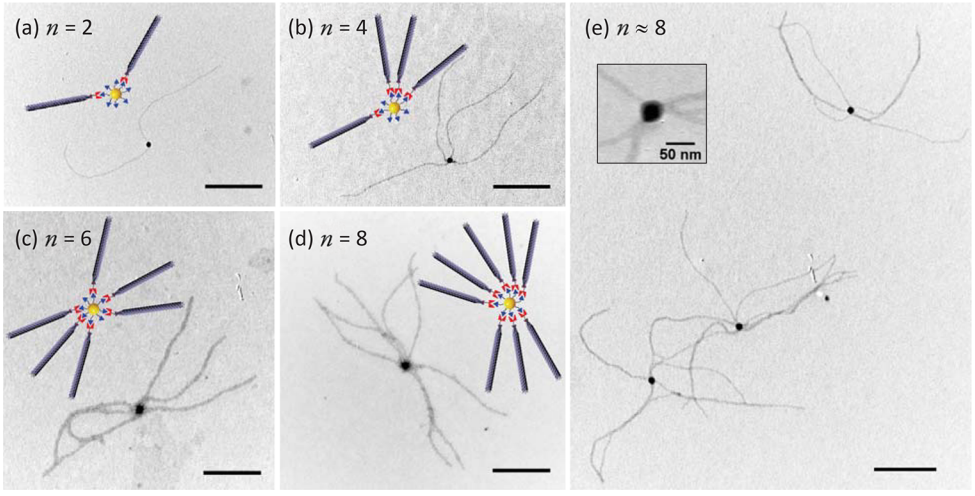

Figure 4. Virus-based multiarm self-assemblies observed by TEM obtained from the reaction between tip-biotinylated phages (M13C7C-B) and streptavidin-coated NPs. The number of arms can be continuously tuned, as illustrated with structures of valency n = 2 ((a), dimer), 4 ((b), tetramer), 6 ((c), hexamer), and 8 ((d), octamer). (e) Large field of view with three multiarm molecules of average valency n = 8. Inset: zoom-in of the multiarm structure core. Except in the inset, the scale bars represent 500 nm.

DOI: 10.1021/acsnano.7b06405
ACS Nano 2017, 11, 10616–10622

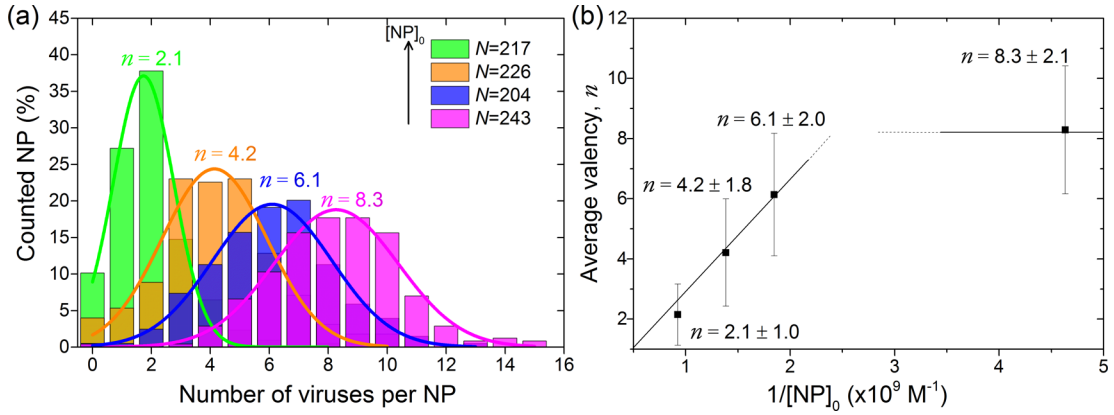

Figure 5. (a) Distribution of the number of viruses per NP for four different samples, at fixed biotinylated virus concentration, $[M13C7C\text{-}B]_0$, and increasing NP concentration, $[NP]_0$. The arithmetic mean, or average valency *n*, is indicated, and the solid lines correspond to Gaussian fits. *N* is the total number of NP counted by TEM for establishing the statistics of each sample. (b) The average valency *n* increases linearly with the molar excess and saturates when *n* reaches the maximum number of available streptavidin proteins per NP, $q \simeq 8$. The error bars are the standard deviation obtained from the Gaussian fits.

particle level by optical fluorescence microscopy (Figure 6), allowing for *in situ*, that is, at equilibrium, sample observation as

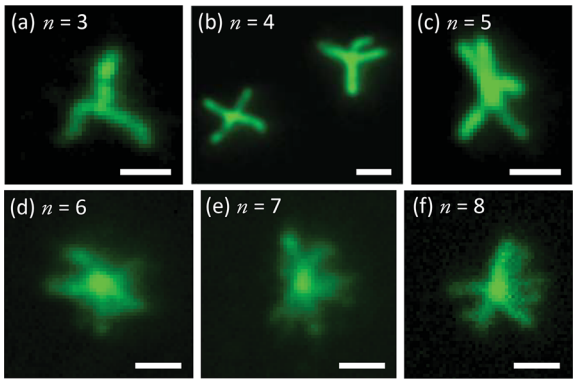

Figure 6. Optical fluorescence microscopy images showing multiarm colloidal molecules formed by fluorescently labeled M13C7C-B phages. Different valencies, *n*, can be observed *in situ* in aqueous dispersions. The scale bar, identical for the six images, represents 1 μm.

shown in the movie presented in Supporting Information. If the structures are identical in shape to those seen by TEM (Figure 4), then the information on the dynamics of the different multiarm structures are available here. Remarkably, some flexibility can be noticed between the arms of the self-assemblies, contrary for instance to multipod structures obtained by crystal growth.[11] This flexibility in the link between bound viruses is distinguishable from the Brownian motion of the multiarm structures themselves. Such *in situ* observations provide the experimental equilibrium state of virus-based multiarm structures.

CONCLUSIONS

In this paper, we have studied the self-assembly of functionalized filamentous viruses into multiarm colloidal structures. First, we used an engineered phage (M13AS), modified at one end to display a polypeptidic sequence (HPQ motif) exhibiting affinity for streptavidin. We determined the dissociation constant of the system in solution to be $K_d = 6 \times 10^{-6}$ M consistent with literature value for this protein tag. In order to strengthen the affinity for streptavidin, a selective and efficient biotinylation protocol of one of the phage tips has been successfully performed. When conjugated with streptavidin activated NPs, these chemically modified phages self-assemble into colloidally stable multiarm structures, whose valency has been continuously tuned from 1 to 8 by varying the molar excess. An additional chemical functionalization of the phage body by fluorescent dyes has been done to optically visualize the multiarm colloidal molecules at the single particle scale and to get *in situ* information on their dynamics. The results presented here show how regio-functionalized viruses can be used as building blocks for mesostructured materials and for the development of a next generation of rod-based colloidal particles.

MATERIALS AND METHODS

M13-AntiStreptavidin phage presents Strep-tags on each of its five p3 proteins localized at one tip. M13AS was kindly provided by S.-W. Lee from the University of California Berkeley (USA). M13AS was isolated through the screening of a phage display library and several rounds of selection for streptavidin, with the following inserted sequence on the p3 proteins, identified by DNA sequencing (see Figure S1 in Supporting Information for the complete sequencing): AC**HPQ**GPPCGGGS.[40] The specific motif histidine-proline-glutamine (HPQ),[35] called Strep-tag, is known for its affinity with streptavidin. Large amplification of these phages of molecular weight $M_w = 1.85 \times 10^7$ g/mol was performed using standard biological procedures.[41] Before further use, M13AS phages were extensively dialyzed against PBS buffer (pH 7.5, I = 20 mM).

A second filamentous phage, called M13C7C and displaying cystein residues on the exposed part of each p3 protein (cystein amino acids otherwise absent from the other coat proteins of the phage), has been used in this study and bioconjugated with maleimide activated biotin. Infecting solution was purchased from New England Biolabs (NEB, USA) and corresponds to a mixture of several M13C7C clones. The amino acid sequences inserted on each of the five p3 proteins of the viruses display seven random amino acids flanked by two oxidized cysteins which form a disulfide bridge. After phage titration, we isolated a plaque consisting of a colony of bacteria infected by a single virus clone and thus a unique amino acid sequence (see Figure S2 in Supporting Information for the complete DNA sequencing). M13C7C phages were also grown and purified using standard biological protocols.[41]

In order to have free thiols available for conjugation with maleimide activated compounds, a reduction step of the disulfide bridges is

DOI: 10.1021/acsnano.7b06405
ACS Nano 2017, 11, 10616–10622

required. This was done by introducing a reducing agent, as Tris(2-carboxyethyl)phosphine hydrochloride (TCEP, Thermo Scientific) used at a concentration around 2 mM.[42,43] To prevent any reoxidization of the free thiols and the reformation of the disulfide bridges, all the reaction process occurred in degassed media and in the presence of 1 mM of ethylenediaminetetraacetic acid (EDTA, Sigma-Aldrich).[42] The viruses were first depleted by the addition of 20% (v/v) of a PEG-8000/NaCl mixture (200 g/L of PEG-8000, 2.5 M of NaCl, degassed), then redispersed in 50 mM Tris (+ 1 mM EDTA, degassed) to have a final concentration of about 1 mg/mL. The dispersion of phages in the presence of TCEP was then stirred (400 rpm) at 4 °C during 48 h.[31,44] After the reduction reaction, viruses were purified by a centrifugation step (13.5 kg during 20 min) followed by 6 rounds of 10 min dialysis against PBS buffer (pH 6.5, I = 350 mM + 1 mM EDTA, degassed). Maleimide-PEG2-biotin (Thermo Scientific) was dissolved in distilled water (maximum solubility: 25 mg/mL). A 1000-fold molar excess was taken per virus and added dropwise to the suspension. The mixture was kept under inert atmosphere thanks to the initial bubbling of argon, protected from light and stirred during 2 h at room temperature. The resulting phages after biotinylation, called M13C7C-B, were then dialyzed against Bis-Tris (I = 20 mM pH 7.4, 0.02% NaN_3) and purified by rinsing with the same buffer in a 100k MWCO filter tube (Amicon Ultra, Merck Millipore).

The fluorescent labeling of the M13C7C-B was achieved in PBS buffer (pH 7.8, I = 350 mM) at a concentration of 0.2 mg/mL. An excess of three dyes (either Alexa488-NHS ester activated, Molecular Probes, or Fluorescein-NHS ester) per p8 main coat protein (about 3000 proteins per virus) first dissolved in *N*,*N*-dimethyleformamide (DMF) was added to the suspension. Particular care was taken that the proportion of DMF does not exceed 20% of the total volume in order to avoid any denaturation of the phages by the organic solvent. The mixture was protected from light and kept under stirring at room temperature during 2 h. The resulting viruses were then extensively dialyzed against Bis-Tris buffer (pH 7.4, I = 20 mM).

To construct multiarm structures with M13C7C-B as well as to estimate the binding affinity of M13AS with streptavidin, the viruses were mixed with 30 nm streptavidin-coated iron oxide NPs (Ocean NanoTech) for 14 h at room temperature. The number of available streptavidin proteins per bead for conjugation with phages, q, is estimated to be of about 8 (maximum mean valency observed). Rather large NPs have been chosen in order to make easier their counting by transmission electron microscopy (TEM) experiments. In particular, nonspecific interactions between viruses can then be easily discriminated, especially when compared with the use of free molecular streptavidin whose relative small size makes tricky its observation by TEM. Note that some streptavidin release occurred with time due to NP aging (lifetime of 3 months).

Samples were then observed by TEM on a Hitachi H-600 microscope operating at 75 kV, and images were recorded with an AMT CCD camera. The diluted virus suspension (typically 10^{-2}–10^{-3} mg/mL) was settled onto freshly treated (O_2 plasma, K1050X, Quorum Technologies) 200-mesh Formvar/carbon-coated grids (Agar), and stained with 2% (w/w) uranyl acetate.

The fluorescent-labeled virus particles were visualized using an inverted microscope (IX-71, Olympus) equipped with high numerical aperture (NA) oil objective (100× PlanAPO NA 1.40, Olympus) and a Neo sCMOS camera (Andor).

ASSOCIATED CONTENT

Supporting Information

The Supporting Information is available free of charge on the ACS Publications website at DOI: 10.1021/acsnano.7b06405.

DNA sequencing of the two bacteriophages and large field of view images by TEM of the control experiment with raw viruses and of the multiarm structures (PDF)

Multiarm colloidal molecules observed by fluorescence microscopy (AVI)

AUTHOR INFORMATION

Corresponding Author

*E-mail: grelet@crpp-bordeaux.cnrs.fr.

ORCID

Eric Grelet: 0000-0002-9645-7077

Author Contributions

‡These authors contributed equally to this work. E.G. designed the project and supervised the research. C.W. and A.C. prepared the biotinylated phages and studied their self-assembly. M.T. prepared the samples and performed the experiments on M13AS viruses. C.W. and A.R. performed the fluorescence microscopy experiments. E.G. and A.C. developed the theoretical model and wrote the manuscript.

Notes

The authors declare no competing financial interest.

ACKNOWLEDGMENTS

This research was supported by the French National Research Agency (ANR) through the project AURORE. We thank Pr S.-W. Lee for the generous gift of M13AS and P. van der Schoot for useful discussion. A.R. acknowledges support from the European Union's Horizon 2020 research and innovation program under the Marie Sklodowska-Curie grant agreement no. 641839.

REFERENCES

(1) Mijatovic, D.; Eijkel, J. C. T.; van den Berg, A. Technologies for Nanofluidic Systems: Top-Down vs. Bottom-Up. A Review. *Lab Chip* **2005**, *5*, 492–500.

(2) Biswas, A.; Bayer, I. S.; Biris, A. S.; Wang, T.; Dervishi, E.; Faupel, F. Advances in Top-Down and Bottom-Up Surface Nanofabrication: Techniques, Applications & Future Prospects. *Adv. Colloid Interface Sci.* **2012**, *170*, 2–27.

(3) Frenkel, D. Order Through Entropy. *Nat. Mater.* **2015**, *14*, 9–12.

(4) van Blaaderen, A. Colloidal Molecules and Beyond. *Science* **2003**, *301*, 470–471.

(5) Manoharan, V. N.; Elsesser, M. T.; Pine, D. J. Dense Packing and Symmetry in Small Clusters of Microspheres. *Science* **2003**, *301*, 483–487.

(6) Wang, Y.; Wang, Y.; Breed, D. R.; Manoharan, V. N.; Feng, L.; Hollingsworth, A. D.; Weck, M.; Pine, D. J. Colloids with Valence and Specific Directional Bonding. *Nature* **2012**, *491*, 51–55.

(7) Salant, A.; Amitay-Sadovsky, E.; Banin, U. Directed Self-Assembly of Gold-Tipped CdSe Nanorods. *J. Am. Chem. Soc.* **2006**, *128*, 10006–10007.

(8) Figuerola, A.; Franchini, I. R.; Fiore, A.; Mastria, R.; Falqui, A.; Bertoni, G.; Bals, S.; Van Tendeloo, G.; Kudera, S.; Cingolani, R.; Manna, L. End-to-End Assembly of Shape-Controlled Nanocrystals *via* a Nanowelding Approach Mediated by Gold Domains. *Adv. Mater.* **2009**, *21*, 550–554.

(9) Huang, Y.; Chiang, C.-Y.; Lee, S. K.; Gao, Y.; Hu, E. L.; De Yoreo, J.; Belcher, A. M. Programmable Assembly of Nanoarchitectures Using Genetically Engineered Viruses. *Nano Lett.* **2005**, *5*, 1429–1434.

(10) Huang, F.; Addas, K.; Ward, A.; Flynn, N. T.; Velasco, E.; Hagan, M. F.; Dogic, Z.; Fraden, S. Pair Potential of Charged Colloidal Stars. *Phys. Rev. Lett.* **2009**, *102*, 108302.

(11) Glotzer, S. C.; Solomon, M. J. Anisotropy of Building Blocks and Their Assembly into Complex Structures. *Nat. Mater.* **2007**, *6*, 557–562.

(12) Manna, L.; Milliron, D. J.; Meisel, A.; Scher, E. C.; Alivisatos, A. P. Controlled Growth of Tetrapod-Branched Inorganic Nanocrystals. *Nat. Mater.* **2003**, *2*, 382–385.

DOI: 10.1021/acsnano.7b06405
ACS Nano 2017, 11, 10616–10622

(13) Cameron, D. J. A.; Shaver, M. P. Aliphatic Polyester Polymer Stars: Synthesis, Properties and Applications in Biomedicine and Nanotechnology. *Chem. Soc. Rev.* **2011**, *40*, 1761−1776.
(14) Kennedy, J. P.; Jacob, S. Cationic Polymerization Astronomy. Synthesis of Polymer Stars by Cationic Means. *Acc. Chem. Res.* **1998**, *31*, 835−841.
(15) He, M.; Pang, X.; Liu, X.; Jiang, B.; He, J.; Snaith, H.; Lin, Z. Monodisperse Dual-Functional Upconversion Nanoparticles Enabled Near-Infrared Organolead Halide Perovskite Solar Cells. *Angew. Chem., Int. Ed.* **2016**, *55*, 4280−4284.
(16) Xu, H.; Pang, X.; He, Y.; He, M.; Jung, J.; Xia, H.; Lin, Z. An Unconventional Route to Monodisperse and Intimately Contacted Semiconducting Organic-Inorganic Nanocomposites. *Angew. Chem., Int. Ed.* **2015**, *54*, 4636−4640.
(17) Feng, C.; Pang, X.; He, Y.; Li, B.; Lin, Z. Robust Route to Unimolecular Core-Shell and Hollow Polymer Nanoparticles. *Chem. Mater.* **2014**, *26*, 6058−6067.
(18) Jiang, B.; Pang, X.; Li, B.; Lin, Z. Organic-Inorganic Nanocomposites *via* Placing Monodisperse Ferroelectric Nanocrystals in Direct and Permanent Contact with Ferroelectric Polymers. *J. Am. Chem. Soc.* **2015**, *137*, 11760−11767.
(19) Yang, D.; Pang, X.; He, Y.; Wang, Y.; Chen, G.; Wang, W.; Lin, Z. Precisely Size-Tunable Magnetic/Plasmonic Core/Shell Nanoparticles with Controlled Optical Properties. *Angew. Chem., Int. Ed.* **2015**, *54*, 12091−12096.
(20) Dujardin, E.; Hsin, L. B.; Wang, C. R. C.; Mann, S. DNA-Driven Self-Assembly of Gold Nanorods. *Chem. Commun.* **2001**, *14*, 1264−1265.
(21) Pal, S.; Deng, Z.; Wang, H.; Zou, S.; Liu, Y.; Yan, H. DNA Directed Self-Assembly of Anisotropic Plasmonic Nanostructures. *J. Am. Chem. Soc.* **2011**, *133*, 17606−17609.
(22) Nie, Z.; Fava, D.; Kumacheva, E.; Zou, S.; Walker, G. C.; Rubinstein, M. Self-Assembly of Metal-Polymer Analogues of Amphiphilic Triblock Copolymers. *Nat. Mater.* **2007**, *6*, 609−614.
(23) Pang, X.; He, Y.; Jung, J.; Lin, Z. 1D Nanocrystals with Precisely Controlled Dimensions, Compositions, and Architectures. *Science* **2016**, *353*, 1268−1272.
(24) Jiang, B.; He, Y.; Li, B.; Zhao, S.; Wang, S.; He, Y.-B.; Lin, Z. Polymer-Templated Formation of Polydopamine-Coated SnO_2 Nanocrystals: Anodes for Cyclable Lithium-Ion Batteries. *Angew. Chem., Int. Ed.* **2017**, *56*, 1869−1872.
(25) Sweeney, R. Y.; Park, E. Y.; Iverson, B. L.; Georgiou, G. Assembly of Multimeric Phage Nanostructures Through Leucine Zipper Interactions. *Biotechnol. Bioeng.* **2006**, *95*, 539−545.
(26) Caswell, K. K.; Wilson, J. N.; Bunz, U. H. F.; Murphy, C. J. Preferential End-to-End Assembly of Gold Nanorods by Biotin-Streptavidin Connectors. *J. Am. Chem. Soc.* **2003**, *125*, 13914−13915.
(27) Gabryelczyk, B.; Szilvay, G. R.; Singh, V. K.; Mikkila, J.; Kostiainen, M. A.; Koskinen, J.; Linder, M. B. Engineering of the Function of Diamond-like Carbon Binding Peptides through Structural Design. *Biomacromolecules* **2015**, *16*, 476−482.
(28) Schaefgen, J. R.; Flory, P. J. Synthesis of Multichain Polymers and Investigation of their Viscosities. *J. Am. Chem. Soc.* **1948**, *70*, 2709−2718.
(29) Pakula, T.; Vlassopoulos, D.; Fytas, G.; Roovers, J. Structure and Dynamics of Melts of Multiarm Polymer Stars. *Macromolecules* **1998**, *31*, 8931−8940.
(30) Molek, P.; Bratkovic, T. Bacteriophages as Scaffolds for Bipartite Display: Designing Swiss Army Knives on a Nanoscale. *Bioconjugate Chem.* **2015**, *26*, 367−378.
(31) Ng, S.; Jafari, M. R.; Derda, R. Bacteriophages and Viruses as a Support for Organic Synthesis and Combinatorial Chemistry. *ACS Chem. Biol.* **2012**, *7*, 123−138.
(32) Cao, B.; Yang, M.; Mao, C. Phage as a Genetically Modifiable Supramacromolecule in Chemistry, Materials and Medicine. *Acc. Chem. Res.* **2016**, *49*, 1111−1120.
(33) Hess, G. T.; Guimaraes, C. P.; Spooner, E.; Ploegh, H. L.; Belcher, A. M. Orthogonal Labeling of M13 minor Capsid Proteins with DNA to Self-Assemble End-to-End Multiphage Structures. *ACS Synth. Biol.* **2013**, *2*, 490−496.
(34) Nam, K. T.; Peelle, B. R.; Lee, S.-W.; Belcher, A. M. Genetically Driven Assembly of Nanorings Based on the M13 Virus. *Nano Lett.* **2004**, *4*, 23−27.
(35) Devlin, J. J.; Panganiban, L. C.; Devlin, P. E. Random Peptide Libraries: A Source of Specific Protein Binding Molecules. *Science* **1990**, *249*, 404−406.
(36) Lee, S.-W.; Lee, S. K.; Belcher, A. M. Virus-Based Alignment of Inorganic, Organic, and Biological Materials. *Adv. Mater.* **2003**, *15*, 689−692.
(37) Kim, W.-G.; Song, H.; Kim, Ch.; Moon, J.-S.; Kim, K.; Lee, S.-W.; Oh, J.-W. Biomimetic Self-Templating Optical Structures Fabricated by Genetically Engineered M13 Bacteriophage. *Biosens. Bioelectron.* **2016**, *85*, 853−859.
(38) Sanders, C. R. *Biomolecular Ligand-Receptor Binding Studies: Theory, Practice and Analysis*; Vanderbilt University: Nashville, TN, 2010.
(39) Green, N. M. *Adv. Protein Chem.* **1975**, *29*, 85−133.
(40) Yoo, S. Y.; Oh, J.-W.; Lee, S.-W. Phage-Chips for Novel Optically Readable Tissue Engineering Assays. *Langmuir* **2012**, *28*, 2166−2172.
(41) Sambrook, J.; Russell, D. W. *Molecular Cloning: A Laboratory Manual*, 3rd ed.; Cold Spring Harbor Laboratory Press: New York, 2001.
(42) Rentero Rebollo, I.; Heinis, C. Phage Selection of Bicyclic Peptides. *Methods* **2013**, *60*, 46−54.
(43) Bellotto, S.; Chen, S.; Rentero Rebollo, I.; Wegner, H. A.; Heinis, C. Phage Selection of Photoswitchable Peptide Ligands. *J. Am. Chem. Soc.* **2014**, *136*, 5880−5883.
(44) Jafari, M. R.; Deng, L.; Kitov, P. I.; Ng, S.; Matochko, W. L.; Tjhung, K. F.; Zeberoff, A.; Elias, A.; Klassen, J. S.; Derda, R. Discovery of Light-Responsive Ligands through Screening of a Light-Responsive Genetically Encoded Library. *ACS Chem. Biol.* **2014**, *9*, 443−450.

DOI: 10.1021/acsnano.7b06405
ACS Nano 2017, 11, 10616−10622

Supporting Information

"Rod-Like Virus Based Multiarm Colloidal Molecules"

Alexis de la Cotte[1,‡], Cheng Wu[1,‡], Marie Trévisan[1], Andrii Repula[1], Eric Grelet[1,*]

[1] *Centre de Recherche Paul-Pascal, CNRS & Université de Bordeaux, 115 Avenue Schweitzer, 33600 Pessac, France*

* grelet@crpp-bordeaux.cnrs.fr

‡ These authors contributed equally to this work

Sequencing results for M13AS (gene 3 reverse complement):

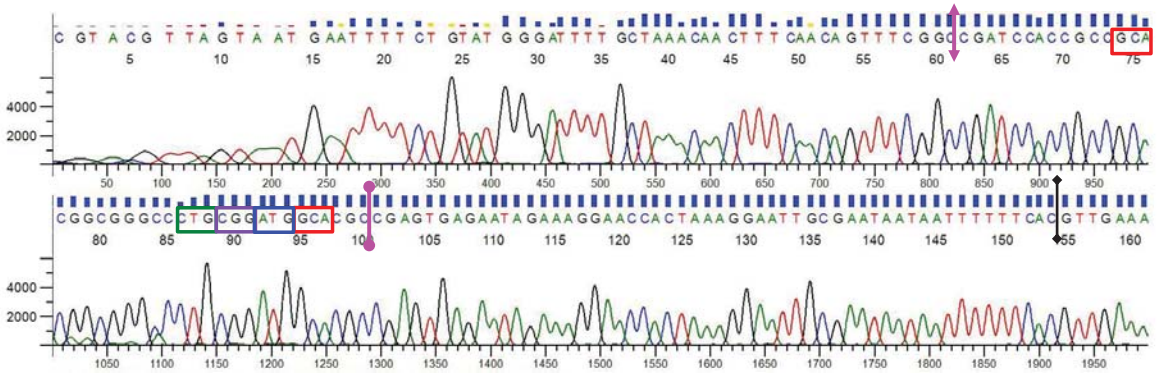

Gene 3 sequence – M13AS:

5′-GTGAAAAAATTATTATTCGCAATTCCTTTAGTGGTTCCTTTCTATTCTCACTCG*GCGTGCCATCCGCAGGGCCC GCCGTGCGGCGGTGGATCG*GCCGAAACTGTTGAAAGT…-3′

p3 protein – M13AS:

N_{ter}-MKKLLFAIPLVVPFYSHS*ACHPQGPPCGGGS*AETVES…-C_{ter}

End of insert in gene 3 complement

Beginning of insert in gene 3 complement

Beginning of gene 3

Cysteine *Histidine* *Proline* *Glutamine*

FIG. S1. DNA sequencing of the gene 3 of M13AS and correspondence of the nucleotide sequence into amino acids. Inserted sequences and amino acids are underlined and italicized.

DNA SEQUENCING OF THE M13AS AND M13C7C PHAGES

The figures S1 and S2 present the DNA sequencing corresponding respectively to the p3 proteins of the M13AS and M13C7C virus strains used in the paper. The sequencings were realized using the toolkit provided by New England Biolabs. The polypeptidic sequences fused to the p3 proteins are ACHPQGPPCGGGS for M13AS and ACNRINHHSCGGGS for M13C7C.

Sequencing results for M13C7C (gene 3 reverse complement):

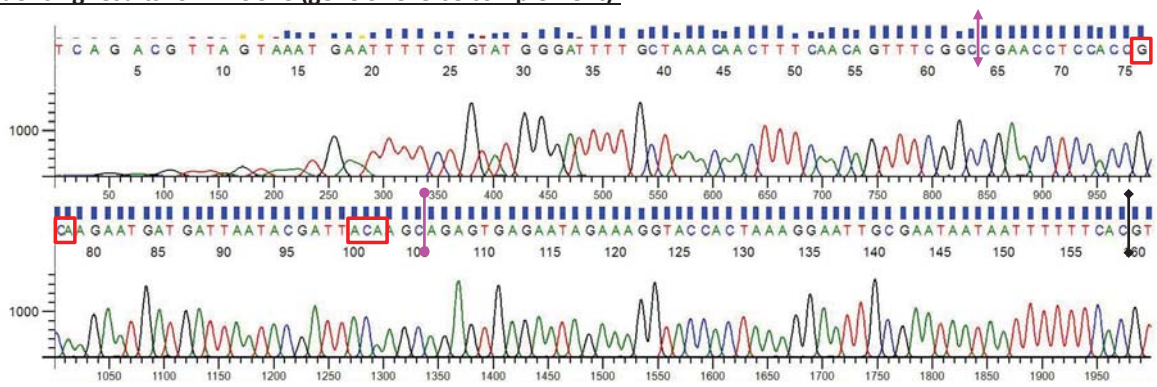

Gene 3 sequence – M13C7C:

5′-GTGAAAAAATTATTATTCGCAATTCCTTTAGTGGTACCTTTCTATTCTCACTCT*GCT**TGT**AATCGTATTAATCAT CATTCT**TGC**GGTGGAGGTTCG*GCCGAAACTGTTGAAACTGTTGAAAGT…-3′

p3 protein – M13C7C:

N_{ter}-MKKLLFAIPLVVPFYSHS*A**C**NRINHHS**C**GGGS*AETVES…-C_{ter}

End of insert in gene 3 complement

Beginning of insert in gene 3 complement

Beginning of gene 3

Cysteine

FIG. S2. DNA sequencing of the gene 3 of M13C7C and correspondence of the nucleotide sequence into amino acids. Inserted sequences and amino acids are underlined and italicized.

FLUORESCENT MOVIES AND LARGE FIELD OF VIEW TEM IMAGES OF MULTIARM COLLOIDAL MOLECULES

The movie has been done by fluorescence microscopy using M13C7C-B phages and displays *in situ* (i.e. in aqueous suspension) dynamics of a three star-like colloidal molecules. The scale bar represents 2 μm.

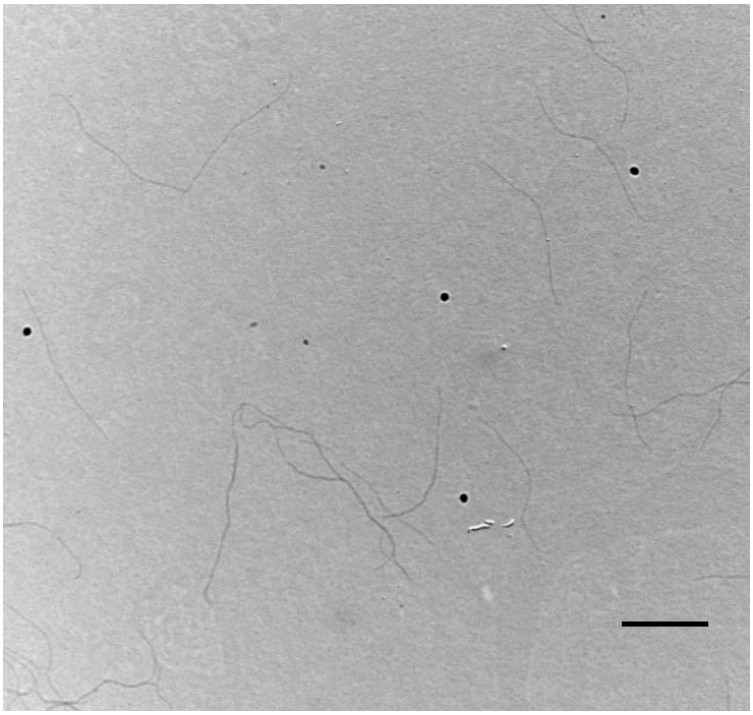

FIG. S3. Control experiment where raw M13 viruses (*without* any tip-functionalization) have been mixed with streptavidin coated beads: no reaction occurred, as demonstrated by TEM. The scale bars represent 500 nm.

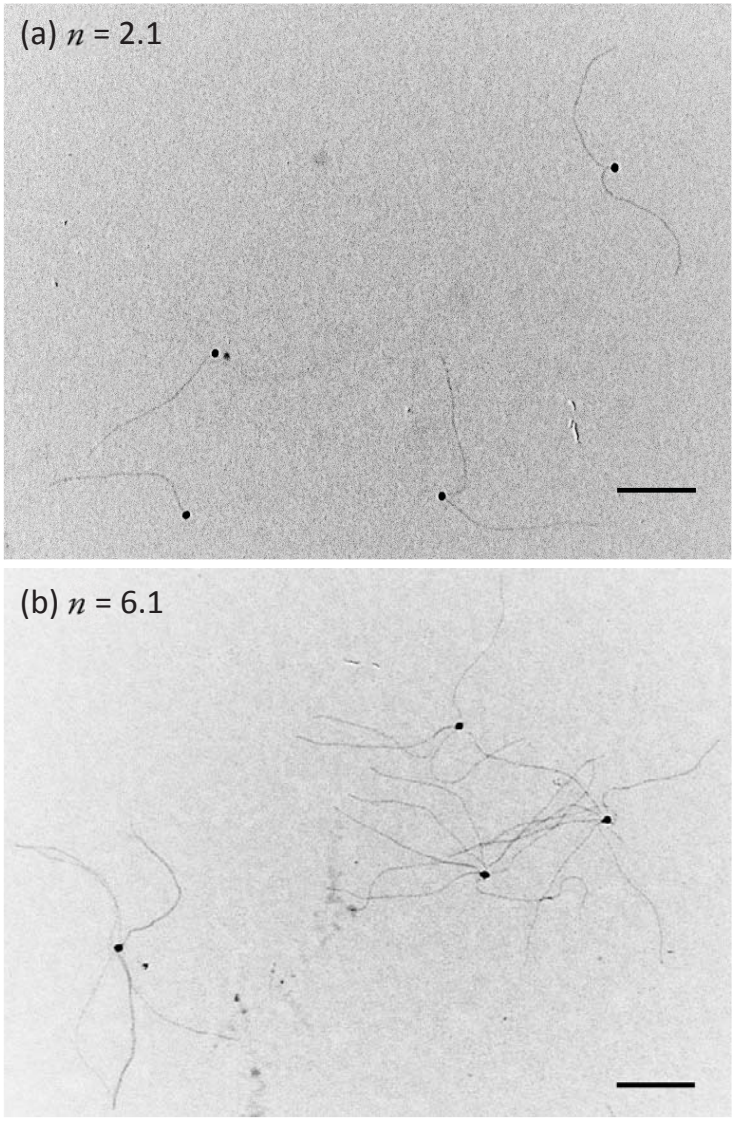

FIG. S4. Large field of view TEM images of biotinylated viruses (M13C7C-B) bound with streptavidin coated nanoparticles, where it can be observed: (a) two multiarm structures of valency $n = 1$ and two multiarm structures of valency $n = 2$ (corresponding to the sample of average valency n=2.1, see main text), (b) four self-assemblies of average valency n=6.1. The scale bars represent 500 nm.